CLOUD CLASSIFICATION AND RAIN-RATE ESTIMATION BY SPATIAL AND SPECTRAL ANALYSIS

Michael J. Uddstrom and Warren R. Gray
National Institute of Water and Atmospheric Research
PO Box 3047, Wellington
New Zealand

1. INTRODUCTION

Clouds and precipitation are expected to play an important role in climate change (Stephens and Greenwald 1991), and in the future will be important for initialising mesoscale prediction systems (e.g. Wright and Golding, 1990). However, establishing characteristics of cloud and precipitation at high spatial resolution remains a problem (e.g. Hou et al. 1993). Over oceanic and data sparse regions this information can, with varying degrees of success, be inferred from passive visible and infrared satellite measurements (e.g. Lovejoy and Austin, 1979; Arkin, 1979; Wu et al., 1985; Rosenfeld and Gutman, 1994). The incidence of cloudy, partially cloudy and cloud free fields of view have been determined by both multi-spectral threshold (e.g. Saunders and Kriebel, 1988; Stowe et al., 1991; and Gutman, 1992) and spatial coherence (Coakley and Bretherton, 1982) methods. More recently, using pattern recognition approaches, cloud morphologies over complex terrain have been estimated from higher order spatial textural information in satellite radiances (e.g. Parikh, 1977; Ebert, 1987; Welch et al., 1988; Tovinkere et al., 1993; Chou et al., 1994). Indeed, Welch et al. (1988), using gray-level co-occurrence textural information alone, indicate that stratocumulus, cumulus and cirrus clouds can be identified using a single LANDSAT TM band. Wu et al. (1985) collocated radar data with geostationary satellite data and by combining spectral and spatial information were able to show that three classes of rain-rate (R), ($R \leq 0.5$ mm h^{-1}, $0.5 \leq R < 5.0$ mm h^{-1}, and $R \geq 5$ mm h^{-1}) could be diagnosed from low resolution infrared and visible imagery of deep convective systems.

However, many reported pattern recognition classification algorithms have been developed from small samples of independent data, with the result that their general applicability is unclear. Welsh et al. (1988) used 12 stratocumulus, 7 cumulus and 2 cirrus cloud field images to specify the spatial characteristics of these cloud classes. Ebert (1987) used 3 Global Area Coverage (GAC) resolution AVHRR polar orbits to determine the characteristics of 18 surface and cloud classes, while Tovinkere et al. (1993) defined a 10 class classifier from data in 6 Local Area Coverage (LAC) AVHRR passes. Wu et al. (1984) derived their rain-rate estimation discriminant functions from 29 GOES-2, GOES-4 and SMS-2 observations spread over three years. While it is possible to label large numbers of cloud class samples from few images, the measurements are clearly not independent, so reducing the number of degrees of freedom in the labelled data. To establish stable class statistics it has been suggested that the sample size for each cloud class should be at least 10 to 20 times the number of classes (Tovinkere et al., 1993).

Labelling or training strategies have also varied – from unsupervised clustering or segmentation (Chou et al. 1994), decision trees (Wu et al. 1985), subjective classification followed by relabelling (of errors) (Garand 1988) and supervised classification (Ebert 1987), to techniques utilising an analyst (Tovinkere et al. 1993). Unsupervised techniques identify features that are separable in the measurement space without recourse to physical interpretation. Cluster classes determined in this way are sensitive to the characteristics of the observing system and the choice of clustering variables. Supervised techniques attempt to define cloud classes known to be associated with particular physical processes such as, stratocumulus cloud capped by a boundary layer inversion, mesoscale organised cumulus, mid-level altocumulus etc. However, with this approach there can be no assurance, apriori, that all such cloud classes will be separable given the satellite measurements.

In the research reported here, a very large sample of LAC AVHRR data has been collocated with radar estimated precipitation at three southern hemisphere maritime midlatitudes locations, where rainfall is dominated

by frontal processes. This sample extends over a year and includes 257 orbits of data. Because of the diversity of this dataset, independence in the training samples is assured, and the data are representative of all seasons. Training samples have been determined for cloud free situations and 7 cloud classes (altocumulus, cirrostratus, cumulonimbus, organised cumulus, nimbostratus, stratocumulus and stratus) using a supervising analyst labelling approach. Finally, it is noted that although AVHRR data have poor temporal resolution (four passes per day, from two spacecraft), compared to geostationary systems, they do have high spatial and radiometric resolution, and sample the atmosphere in 5 wavelength regions. Consequently it is expected that an optimal pattern recognition, rather than decision tree cloud classification scheme might be developed from these data, and the relationships between the high resolution radiometric, spatial and radar precipitation data investigated.

2. DATA

The areas for which data have been collected are shown in Fig. 1 and are centred on the sites of the three S-Band radars, Mt. Tamahunga (36.30°S, 174.71°E at 453 m above mean sea level (amsl)), Outlook Hill (41.31°S, 174.64°E at 534 m amsl) and Rakaia (43.79°S, 172.02°E at 124 m amsl). Each area is 480 km square, corresponding to the radar's maximum range of 240 km.

2.1 Satellite Data

The AVHRR instruments used here (NOAA11 and NOAA12) are five channel devices, having nominal spectral intervals:- 0.55 - 0.68 μm (1); 0.725 - 1.1 μm (2); 3.55 - 3.93 μm (3); 10.5 - 11.5 μm (4), and 11.5 - 12.5 μm (5). These channels provide measurements from the visible (i.e. 1 and 2), near infrared (i.e. 3) and infrared (i.e. 4 and 5) parts of the spectrum. The data are at LAC spatial resolution, yielding an instantaneous field of view (ifov) of 1.1 km at nadir, and are stored and analysed at 10 bit (full) radiometric resolution.

Channel 1 and 2 bi-directional reflectances of the scene were calculated using the pre-launch calibration coefficients and a correction for the solar view angle (equ 1).

$$R_n = \frac{G_n C + Y_n}{\cos\theta} \qquad (1)$$

Here R_n is the bi-directional reflectance for channel n, G_n and Y_n are the gain and intercept (from Appendix B of Planet, 1989), C is the raw count value, and θ the solar zenith angle at the ifov.

The longwave thermal channels were calibrated using the non-linear method given in Planet (1989). Thermal difference ($T_4 - T_5$, $T_4 - T_3$) channels were also computed – the latter for night time data only. For daytime data, a visible ratio channel (v_2) was computed using the approach suggested by Gutman (1992).

$$v_2 = \frac{R_2}{R_1} - 1 \qquad (2)$$

This quantity is equivalent to the definition of the Normalised Difference Vegetation Index (NDVI) and has a value near zero for cloud.

Regions of sunglint, or specular reflection, were identified through examination of the sun – ifov – sensor geometry using the method of Stowe et al. (1991), who calculate the angle γ (equ 3)

$$\gamma = \cos^{-1}[\cos(z_0)\cos(Z) + \sin(z_0)\sin(z)\cos(A)] \qquad (3)$$

where z_0 and z are the solar and satellite zenith angles (as viewed from the field of view) and A is the relative azimuth angle between the sun and the satellite. Here, sunglint is assumed whenever γ is less than 15 degrees.

The AVHRR data are remapped onto Lambert Conformal projections at 1 km resolution and full radiometric resolution.

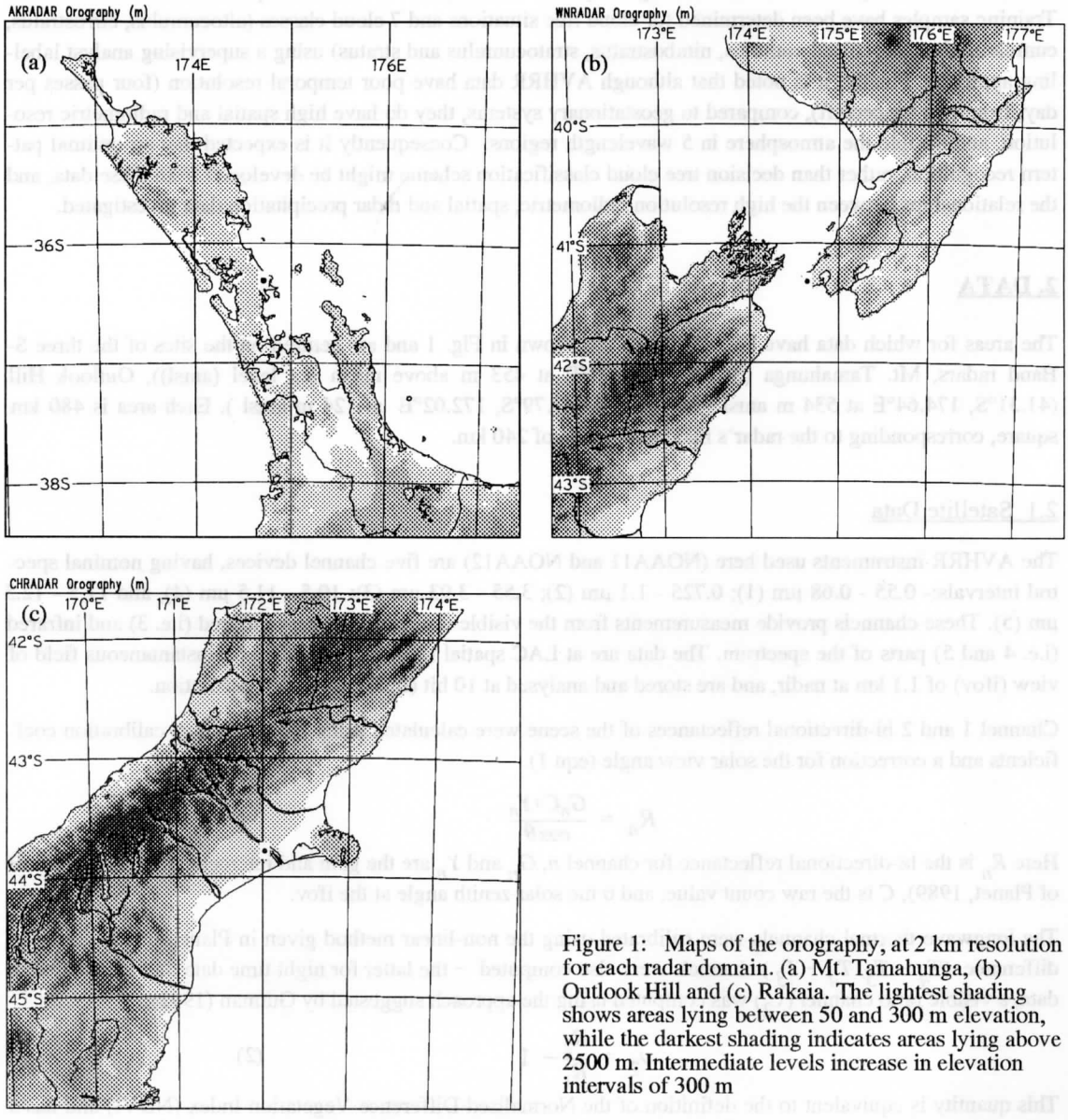

Figure 1: Maps of the orography, at 2 km resolution for each radar domain. (a) Mt. Tamahunga, (b) Outlook Hill and (c) Rakaia. The lightest shading shows areas lying between 50 and 300 m elevation, while the darkest shading indicates areas lying above 2500 m. Intermediate levels increase in elevation intervals of 300 m

2.2 Radar Data

All three radars operate at a wavelength of 5.6 cm, have nominal beam widths of 0.86°, 2 km range bins and are controlled by Ericsson Weather Information System (EWIS) software. They generate polar-volume scans at 10 elevations, the lowest four of which are 0.5°, 0.9°, 1.3° and 2.5°. Full volume scans are carried out every 15 minutes and take 2 minutes to acquire. Post processing of these data allow corrections to be estimated for errors induced by hill and sea clutter, attenuation, beam blocking and the vertical profile of reflectivity effects. Rain-rates were calculated using the standard Z-R relationship for frontal rain ($Z\ (mm^6\ m^{-3}) = 200\ R^{1.6}$), and rectified onto the same grid as that used for the satellite data

Ground and sea-wave clutter were identified through their vertical and horizontal structure signatures. Wave clutter shows a rapid decrease of reflectivity with height, while hill clutter can be identified by comparing the horizontal reflectivity patterns over 5 * 5 tiles (centred on the target) with those arising from the topography's height and slope. This approach is used, since hill clutter tests based on Doppler data often fail owing to tree-

motion induced signals. Beam blocking effects were corrected by estimating the fraction of the beam blocked by the hills, assuming propagation effects can be modelled using the 4/3 Earth approximation and the antenna pattern by a sinc function. The attenuation correction algorithm used was iterative and similar to that of Hildebrand (1978), where the attenuation per kilometre is estimated from the measured rain-rate R (mm h^{-1}). Finally, the precipitation at the surface must be inferred from radar measurements sampling precipitation at some range-dependent height above the Earth's surface. Since the vertical profile of reflectivity (VPR) varies in both space and time a model, of the VPR is first estimated using an approach similar to that of Gray (1991), where the average (spatial) VPR is estimated from the radar volume scan data.

Although much effort has been put into quality controlling the radar data, possible errors in the surface reflectivity estimate of 1-2 dB could still be present (Austin 1987). An underestimate of 2 dB at a reflectivity of 37 dBZ (a 5% error) represents an increase in rainfall rate of 7.5 to 10 mm h^{-1}. Also since the terrain around the radar sites is rugged (see Fig. 1) it is not always possible to remove all hill clutter effects, consequently these areas were avoided in the following analysis.

3. METHODOLOGY

Pattern recognition algorithms are highly dependent upon the span of the data utilised in the training (or labelling) phase, and on the training method employed. In this study samples have been drawn from 105 NOAA11 and 152 NOAA12 passes during the period 14 December 1993 to 31 November 1994.

The training (or sample labelling) strategy pursued here is to use an analyst to identify (or label) specific cloud classes on any particular image. To enable the analyst to accurately label cloud samples a comprehensive set of diagnostic tools was provided.

3.1 Spatial Characteristics

The spatial, or textural characteristics of an image can be described by specifying statistical measures of the distribution of "gray levels" in an image. Weszka et al. (1976) carried out a comparative study of a number of texture measures, including Fourier power spectrum analysis, second-order gray-level statistics, gray-level difference statistics, and gray-level run length statistics. They found that features described by both the second-order and difference statistics were best able to separate terrain features, and that the accuracy of these two methods was essentially identical. Since the gray-level difference method is computationally less expensive than the second order method, it has been chosen for this work.

Gray-level difference (GLD) statistics measure the local properties of the absolute differences between pairs of gray-levels in an $n \times n$ pixel image area. A GLD probability density function for the image can be defined, and has the form $P(m)_{d,\theta}$ where the m th entry is the relative frequency of occurrence of gray-level difference $m = |i - j|$ for pixels separated by d pixels in direction θ (relative to the horizontal). If the texture is coarse, relative to distance d, then the differences m might be expected to be small and $P(m)_{d,\theta}$ will be large for small m, and small for large m. Conversely, for fine texture, where d is comparable to the scale of the features in the image, $P(m)_{d,\theta}$ will be large for large m. Accordingly, measures of the texture in an image may be computed from estimates of the spread in $P(m)$ at different separations and angles. Conventionally four measures are utilised, where $m = |i - j|$, and N is the number of gray-levels :-

1. The mean, equ. (4):-

$$\mu_{d,\theta} = \sum_{m=0}^{N} m P(m)_{d,\theta} \qquad (4)$$

which, if small, indicates that the GLD values are concentrated near the origin (i.e. m=0) and the texture is "coarse" relative to the spatial scale d.

2. The contrast, equ (5):-

$$CON_{d,\theta} = \sum_{m=0}^{N} m^2 P(m)_{d,\theta} \qquad (5)$$

or second moment of the $P(m)$ density function, measures the variability of the gray levels in the image.

3. The angular second moment, equ (6):-

$$ASM_{d,\theta} = \sum_{m=0}^{N} [P(m)_{d,\theta}]^2 \qquad (6)$$

which measures the degree of homogeneity in the image. A small ASM implies that the gray-level differences are all similar and the sampled area has textural variations on a spatial scale close to d, whilst a large ASM indicates that there are dominant gray tones present (e.g. when the GLD values are concentrated near m=0).

4. The entropy, equ (7):-.

$$ENT_{d,\theta} = -\sum_{m=0}^{N} P(m)_{d,\theta} \log P(m)_{d,\theta} \qquad (7)$$

This parameter indicates whether the "texture" is organised. This is largest when the $P(m)$ are equal, or randomly distributed, but is small when they are very unequal.

Each parameter is computed at four angles (θ = 0°, 45°, 90° and 135°), and any number of pixel separations d while directionally averaged measures of texture are computed by averaging the parameters over all four directions.

The GLD statistics are nominally defined on gray levels (or counts), however, calibrated binned physical variables are used here. This approach ensures that the textural characteristics from different NOAA series spacecraft may be combined together.

Table 1: Features computed for all data (including difference and ratio satellite channels, and radar data)

Feature Number	Feature Description	Feature Number	Feature Description
1	Mean	10	Minimum GLD Contrast
2	Minimum	11	Maximum GLD Contrast
3	Maximum	12	Directionally averaged GLD ASM
4	Standard Deviation	13	Minimum GLD ASM
5	Average Roberts Gradient	14	Maximum GLD ASM
6	Directionally averaged GLD mean	15	Directionally averaged GLD Entropy
7	Minimum GLD mean	16	Minimum GLD Entropy
8	Maximum GLD mean	17	Maximum GLD Entropy
9	Directioanlly averaged GLD Contrast	18 – 33	Four (θ) components of all GLD statistics

3.2 Training Strategy

The analyst is provided an interactive tool (called ENHANCE (see Kidson et al. 1992)) to diagnose cloud types in some image. ENHANCE allows the primary data sources (i.e. the AVHRR and radar data) to be viewed, standard enhancement curves modified to bring out specific features (e.g. by histogram equalisation), sub-areas enlarged, and vector fields, such as radar rain-rate overlaid. Difference and ratio channels (e.g.($T_4 - T_3$), ($T_4 - T_5$), v_2) may also be displayed. Centring the cursor on some cloud of interest, results in the calcu-

lation and display of the spectral and spatial characteristics of an 8 × 8 (or 16 × 16, or 32 × 32), pixel square area surrounding the cursor. The characteristics displayed include:-

- single and multi-variable histograms of all data, including radiances, and derived channels.
- Breatherton Coakley (Molnar and Coakley, 1985) spatial coherence plots and channel by channel plots on 2 × 2 tiles within the 8 × 8 selected areas
- the features noted in Table 1 (for all data, including radiances and derived channels).

From these diagnostics, single layer clouds are classified according to the meteorological situation and the approximate constraints noted in Table 2. This procedure has been called SRTex (Satellite Rainfall by Texture)

Table 2: Cloud type labelling rules for SRTex classification

Cloud Class	Name	Characteristics			
St	Stratus	Rain $(T_4 - T_5)$ $(T_4 - T_3)$ (Night)	No Positive Positive (> 0.5°C)	T_4 R_3 (Daylight) Dimension	Warmer than 0 °C High Large area
Ns	Nimbostratus	Rain $(T_4 - T_5)$ T_4 range	Yes (no for As) Positive −1 to −30 °C	Dimension	Large area Includes non-raining altostratus
CiC	Cirrus over Cloud	Rain $(T_4 - T_5)$	Allowed Positive (> 0.5 °C)	T_4 Dimension	< −25°C Linear structure, underlying clouds evident (or raining).
Sc	Stratocumulus	Rain $(T_4 - T_5)$ T_4	Possible Positive Warmer than 0 °C	Dimension	Large area - granular
Ac	Alto-cumulus	Rain $(T_4 - T_5)$	Less than 5 mm h^{-1} Near zero	Dimension	Large
Cu	Cumulus	Rain $(T_4 - T_5)$	Not necessary Maybe negative, or near zero	Dimension	Of the order of 10–20 km, (e.g. squall line, open-cell, embedded)
Cb	Cumulonimbus (isolated)	Rain $(T_4 - T_5)$ Cirrus shield	> 6 mm h^{-1} Negative or near zero Present	Dimension	Greater than 20 km
NC	No Cloud				

The climatological sea surface temperature for the selected area and housekeeping information such as the area's location, the satellite characteristics, and an analyst identifier, are saved along with the satellite, and radar data.

Altogether 257 collocated radar and satellite images were examined, spanning all seasons, leading to a combined training set of 4323 samples - certainly large enough to satisfy sampling constraints for an 8 class discriminant function..

4. Cloud Characteristics

Tukey box plots (Tukey, 1977) of cloud class characteristics of T_4 (sample mean, GLD mean, and entropy), $(T_4 - T_5)$(mean), $(T_4 - T_3)$(mean) and v_2 (mean) are given in Fig.1 below.

While this figure includes interesting detail, the main points might be summarised as follows:-

- While the T_4 mean (Fig 1a) does not discriminate cirrus and cumulonimbus classes, the GLD texture measures do (e.g. Fig 1b). The cumulonimbus is expected to include a cirrus shield, but this is transmissive with the result that the cumulonimbus remains much "grainier" than cirrostratus, and is therefore separable.
- The lowest GLD means (Fig 1b), indicating coarse texture relative to the GLD separation parameter, d, are associated with those classes having the lowest expected spatial structure (i.e. classes NC and St).
- The Entropy statistic (Fig 1c) confirms that the no cloud (NC) and more stratiform clouds (i.e. St, Sc, CiC) show the most "organised" structure while the cumuliform clouds show the least.

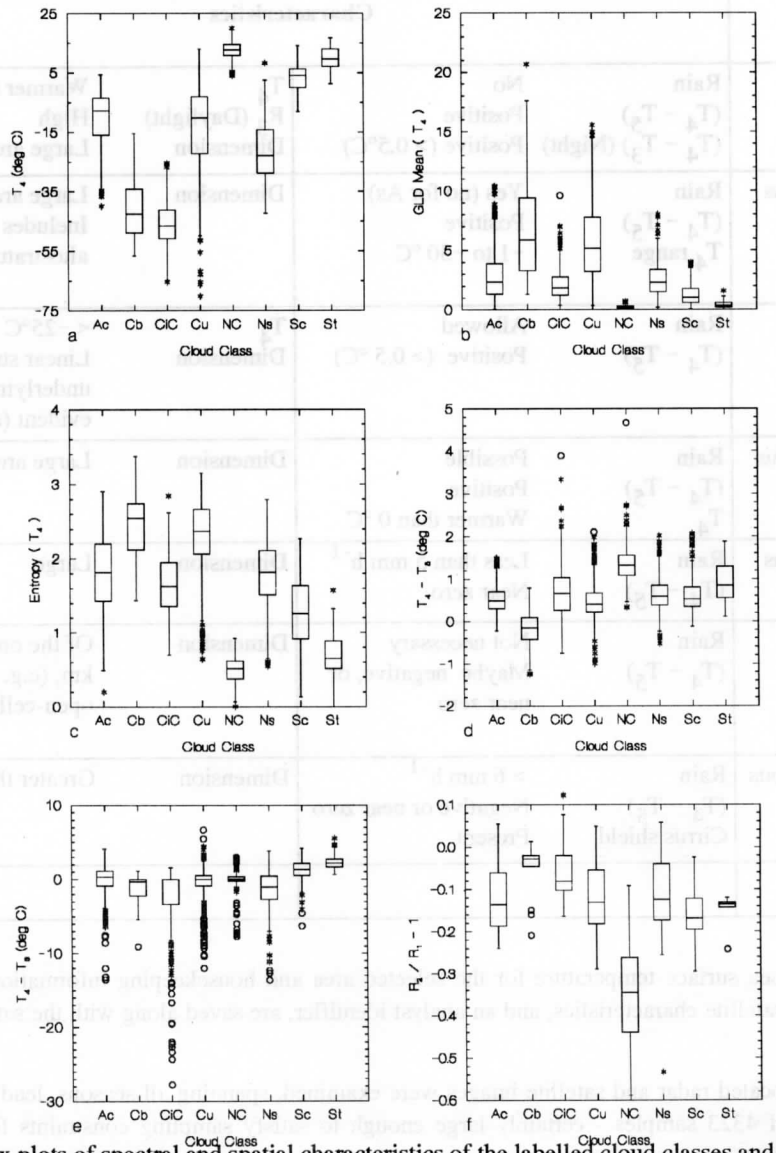

Figure 1: Box plots of spectral and spatial characteristics of the labelled cloud classes and 8 × 8 pixel samples. (a) Mean T_4 temperature, (b) GLD Mean T_4, (c) GLD entropy T_4, (d) Mean $(T_4 - T_5)$, (e) Mean $(T_4 - T_3)$ (night time data) and (f) v_2 mean. The horizontal line in the "box" represents the sample median and the upper and lower ends of the box are the hinges or medians of the remaining halves of the data. The whiskers are 1.5 times the absolute difference between the respective hinge and median, and all outliers are represented by either asterisks or small circles (i.e. greater than 3 times the absolute difference between the median and respective hinge.)

- The textural characteristics of stratus are very similar to those of the no-cloud class at a GLD separation (d) of one pixel (i.e. 1.1 km). However during night hours stratus is detectable radiometrically. The temperature difference ($T_4 - T_3$) (Fig 1e) is positive for opaque water clouds since their emissivity at 3.7 μm is near 0.8, while at 11.5 μm it is close to 1.0 (Hunt 1973). The ν_2 data provide a similar capability during daylight hours. For cirrus clouds, the difference has the opposite sign, and may be quite large due to transmission through the cloud (Olsen and Grassl 1985). These differences can, however, be confounded when the temperature varies across an ifov (e.g., a partially cloud filled) since the 3.7 μm radiance is about three times more sensitive to temperature changes than the 11 μm radiance.
- For low clouds and no-cloud ($T_4 - T_5$) (Fig 1d) is positive and provides a measure of the amount of water vapour above the cloud / surface. Cirrus clouds also yield positive ($T_4 - T_5$) differences since the emissivity of cirrus at 11 μm is lower than at 12 μm (Inoue, 1987) albeit at lower temperatures (T_4 or T_5).
- The ratio channel ν_2 (Fig 1f) is related to Saunder's and Kriebel's Q, since $\nu_2 = Q - 1$, (Saunders and Kriebel, 1988) and for the labelled cloud classes shows characteristics similar to those described by these authors.

These results suggest that the spatial parameters can be usefully employed in the cloud classification problem since they provide information not present in the radiative measures when treated independently.

Probability plots (not shown) of the radiative and textural data by day / night separation indicated no day / night signal in the thermal channels, as would be expected from samples over the sea. As a result of using calibrated data no significant intersatellite differences were detected.

5. CLOUD TYPE DISCRIMINATION

Using the radiative and texture characteristitics of a sufficiently large sample of cloud classes identified in the training, or labelling stage, a Bayesian discriminant function can be developed to classify cloud classes in independent data. This approach while utilising all available information such as the span of each class, its expected probability of occurrence, and the feature vector mean and covariance structure, does assume that the underlying probability distribution is of known form. When that distribution is multivariate Gaussian, and the measurement errors are unbiased, then a measure of the distance between a given (observed) feature vector, **f**, and the i th cloud class, $g_i(\mathbf{f})$ is:-

$$g_i(\mathbf{f}) = log[P(\omega_i) \,/\, (2\Pi^{\frac{m}{2}} \,|\, \mathbf{S}_{fi} \,|^{\frac{1}{2}})] - \tfrac{1}{2}(\mathbf{f} - \bar{\mathbf{f}}_i)^T \mathbf{S}_{fi}^{-1} (\mathbf{f} - \bar{\mathbf{f}}_i) \quad (8)$$

where **f** is the feature vector of radiative and spatial data (dimension m), $P(\omega_i)$ the *a priori* probability of occurrence for the i th cloud class, and $\bar{\mathbf{f}}_i$ and S_{fi} the associated class mean and covariance. The *a posteriori* probability of the observed feature vector belonging to the i th class of N possible classes is just:-

$$p(\omega_i \,|\, \mathbf{f}) = exp(g_i(\mathbf{f})) \,/\, \sum_{j=1}^{N} exp(g_j(\mathbf{f})) \quad (9)$$

and the expected class membership can be estimated by determining the class (i) that maximises the probability $p(\omega_i \,|\, \mathbf{f})$ ($i = 1, N$) of equ 9.

The accuracy of the discriminant function estimator is dependent upon; the number of classes to be identified, their expected probability of occurrence, the class separability in feature vector space (including choice of fea-

ture vector elements), and "measurement" noise. Some classification errors are inevitable, since the labelling process utilised information not available to the discriminant function, such as cloud extent and relationships to synoptic features. However, in other cases, cloud classes will have significant overlap in feature space due to their similar physical origins. In these cases, e.g. the altocumulus and cumulus classes, misclassifications will occur but are not be expected to have high cost.

5.1 Night Equations

A number of discriminant function models were investigated and the results given in Table 7, where the skill of each model is summarised by the fraction of correct classifications, the Kuiper's skill score (see Murphy and Katz, 1985), and the Probability of Detection (POD) of the cumulus, no-cloud and stratus classes. Generally, the inclusion of spatial statistics increases the skill of the discriminant function considered across all eight classes. However, a more detailed examination of the results can be performed by considering the POD values for the three "cloud" classes noted.

Table 3: Discriminant function model skill characteristics for 8 class (Ac, Cb, CiC, Cu, NC, Ns, Sc, St) classification of nighttime data using equal prior probabilities, i.e. $P(\omega_i) = 0.125$. POD is the Probability of Detection.

Model id	Feature Vector	Fraction Correct	Kuiper's Index	POD Cu	POD NC	POD St
1	T_4, $(T_4 - T_5)$	0.521	0.454	0.15	0.74	0.40
2	T_4, $(T_4 - T_3)$	0.576	0.508	0.14	0.93	0.69
3	T_4, $(T_4 - T_5)$, *ent* (T_4)	0.630	0.577	0.60	0.77	0.49
4	T_4, $(T_4 - T_5)$, $(T_4 - T_3)$	0.561	0.492	0.18	0.83	0.47
5	T_4, $(T_4 - T_5)$, $(T_4 - T_3)$, *ent* (T_4)	0.666	0.614	0.61	0.85	0.55
6	T_4, $(T_4 - T_5)$, $(T_4 - T_3)$, *ent* (T_4), $\mu\ (T_4 - T_5)$	0.673	0.621	0.58	0.86	0.54
7	T_4, $(T_4 - T_3)$, *ent* (T_4)	0.676	0.620	0.59	0.94	0.61
8	T_4, $(T_4 - T_3)$, *ent* (T_4), $\mu\ (T_4 - T_5)$	0.684	0.629	0.57	0.93	0.59
9	T_4, $(T_4 - T_3)$, *ent* (T_4), $\mu\ (T_4 - T_5)$, *con* (T_4)	0.681	0.628	0.46	0.91	0.56

Comparison of the NC and St PODs from models 1 and 2 shows that use of the radiative information in the T_3 temperature significantly improves the skill of the discriminant function. The reduction in stratus misclassifications observed in Table 3 may seem less than might be anticipated from consideration of the radiative information only - especially when compared with rule based, threshold driven cloud classification schemes such as CLAVR (Stowe et al 1991), MAGIC (Gutman 1992) and APOLLO (Saunders and Kriebel, 1988). However the Bayesian discriminant function finds the most likely class based on the information in *all* feature vector components simultaneously. Addition of the T_4 entropy spatial statistic to the T_4 and T_5 model (cf. models 1 and 3) leads to only small improvements in skill. However, adding the T_4 entropy to the T_4 and T_3 model (cf. models 2 and 7) degrades the skill of the discriminant function in regard to POD of NC and St classes. Those cloud classes (St and Sc) most likely to be misclassified as NC all have similar spatial characteristics (i.e. low mean (μ), contrast and entropy, and high Angular Second Moments) as noted in Fig. 1. The improvements in the POD for the NC class are necessarily mirrored in the POD values for the St class. Clearly, when the spatial or textural characteristics are similar, the radiative information dominates.

When the POD values for the mid to high level Cumulus class are examined, as well as the Kuiper's Index for the skill of the discriminant function over all classes, it is clear that the use of spatial statistics significantly improves the skill of the discriminant function models. A number of other feature vector models were tried, including those using the minimum, maximum and range statistics of the basic and GLD directional statistics. Although Wu et al. (1985) found these to be of primary importance for identifying raining regions in deep convective clouds, use of these measures did not improve the skill of cloud discrimination functions.

5.2 Day Data

Daytime equations were derived from those data having local solar zenith angles less than 81.5° and lying outside the sunglint region (i.e. $\gamma > 15°$). The v_2 ratio channel alone can detect the no-cloud class with some skill, but it has little skill at discriminating cloud type. As additional features are included, the skill of the discriminant function improves to values that are the similar to those for the night data

6. RAIN-RATE ESTIMATION

To examine the relationships between the collocated rain-rate and satellite measurements, those data where the time difference between observations is greater than 10 minutes were excluded, as were rain-rate samples inferred from data above the bright band. The hypothesis that the within class variance in rainrate could be estimated from the multi-spectral and spatial information in the AVHRR measurements was then examined using standard stepwise multivariate (linear) regression methods. In the best case, altocumulus, 25% of the variance (adjusted R^2) could be explained using T_4 predictors [1][1], [2], [7], [8], [16], and [17], and ($T_4 - T_5$) predictors [1], [3] and [16]. These features provide estimates of cloud top temperature, cirrus or water-vapour contamination, and provide a measure of the vertical development in the clouds. However in the worst case, cirrostratus, only 10% of the rain-rate variance could be explained using stepwise linear regression methods. This result is not surprising though, since the rain processes are largely decoupled from the overlaying cirrostratus.

To determine whether the rain-rate estimation skill was limited by the assumption of linearity, non-linear interactions were considered. The class spectral and spatial data were clustered using an unsupervised method (K-Means). Given some desired number of classes, this approach maximises the between cluster to within cluster variation. Clustering on the most significant variables identified in the stepwise regression, the altocumulus data were divided into two subsamples. The mean rain-rates associated with these sub-samples were 0.6 and 1.2 mm h^{-1}, and are significantly different at the 99.5% confidence level. The lower rain rate cluster is associated with warmer temperatures, lower entropy and little directionality in the T_4 GLD mean. The nimbostratus class showed similar separability in rain-rate.

An alternative approach is to attempt to determine whether there is sufficient information in the satellite data to delineate the rain and non-raining parts of clouds (e.g. see Lovejoy and Austin, 1979). To test this hypothesis the data were grouped into rain and no-rain sub-classes and significance tests of the rain / no-rain differences computed for all features noted in Table 1. Cloud class specific Bayesian discriminant functions were estimated from the most significant, independent data using prior probabilities ($P(\omega_i)$) determined from the rain / no-rain frequency characteristics of each class.. The resultant feature vectors, and fraction of correctly classified data are given in Table 4. Owing to sample size limitations, no results are given for the cumulonimbus class.

Table 4: Rain / no-rain feature vectors and skill scores. The item in the {.} braces refers to the entries in Table 1 .

Cloud Class	Prior Probability		Feature Vector	Fraction Correct
	Rain	No-Rain		
Ac	0.53	0.47	T_4[17], T_4[12], T_4[16], T_4[7], T_4[8], ($T_4 - T_5$)[7]	0.64
Cb	n/a			
CiC	0.50	0.50	($T_4 - T_5$)[3]	0.60
Cu	0.07	0.93	T_4[2]	0.93
Ns	0.18	0.82	T_4[6], T_4[7], T_4[8], T_4[9], T_4[2], T_4[3]	0.85

[1] See Table 1 for definition of features.

Evidently, for cumulus cloud, the cloud top temperature may be used to delineate regions in the cloud where rain is reaching the surface, although the accuracy of this prediction is low since nearly all the labelled cumulus clouds in the sample were precipitating. However the feature vectors identified for the altocumulus, cirrostratus and nimbostratus all demonstrate positive skill at delineating rain / no-rain regions in cloud.

Interestingly, while rain / no-rain areas in cumulus could be delineated using cloud top temperature, in the other classes classes, cloud top temperature is either not related to the delineation of rain / no-rain areas (e.g. cirrostratus) or is weakly linked. For altocumulus and nimbostratus, the most significant features are of a spatial nature.

7. CONCLUSIONS

Based on analysis of an extensive, 257 orbit, 12 month sample of AVHRR LAC data, there is good evidence that 8 × 8 km resolution scenes can be classified into altocumulus, cumulonimbus, cirrostratus, cumulus, nimbostratus, stratocumulus, stratus and no-cloud classes with significant skill (Kuiper's skill scores of the order of 0.63). Using equal prior probabilities, the percentage of samples correctly classified is of the order of 70% (over all classes) for a discriminant function utilising 3.7 (T_3), 11 (T_4) and 12 μm (T_5) temperatures, GLD contrast, entropy and mean spatial textural features. Excluding the spatial information reduces the percent correctly classified to 56%, and the skill score to 0.49. Although these results are for dependent data, given the size and span of the samples it is unlikely that the results will differ greatly when applied to independent data.

Although it is true that adding the spatial information does improve the overall accuracy of the discriminant function, some cloud types are more reliant upon this information than others. For example the radiometric information is the most important component for discriminating stratus and cloud free scenes, since the spatial statistics for these classes are quite similar and there is a a strong radiometric signal in the infrared measurements. However, for upper level stratiform and cumuliform clouds the information in the spatial statistics is significant.

Results from attempts to model rain-rate from the satellite radiometric and spatial data show mixed results. The cloud classification algorithm is able to discriminate raining (altocumulus, cumulus, cumulonimbus, cirrostratus and nimbostratus) from non-raining classes (stratus and stratocumulus), although these classes could also be delineated using simple temperature threshold methods. For raining classes, it has also been possible to show that the rain / no-rain samples can be delineated with some skill, and that the most useful features for this purpose are not generally radiometric. In such cases the degree of directionality in the GLD statistics of the radiometric data is important. Within class rain-rates can also be modelled for the altocumulus and cumulus classes, at the level of 20 to 25% explained variance. For both these classes, the sets of GLD statistics which measure the spatial structure in the data are important predictors.

While these results do not verify those presented by Wu et al. (1985), it should be noted that they concentrated on deep convective systems, which tend to have well defined growth and decay phases. These phases might also be expected to be reflected in there textural characteristics, and hence improve the skill of the rain-rate discrimination algorithm. The data sets used here reflect the characteristics of mid-latitudes frontal rain, which are clearly different.

Acknowledgements The authors extend grateful thanks to Jonathon Couper and John Kidson for significant help with the software required to give the ENHANCE image processing system the capability to provide an optimised labelling environment for the classification of cloud imagery.

8. REFERENCES

Austin, P. 1987: Relationship between measured radar reflectivity and surface rainfall. *Mon. Wea. rev.*, **115**, 1053 - 1070.

Arkin, P.A., 1979: The relationship between fractional coverage of high cloud and rainfall accumulations during GATE over the B-scale array. *Mon. Wea. Rev.* **107**, 1382 - 1387.

Chou, J., R.C. Weger, J.M. Lightenberg, K.-S. Kuo, R.M. Welch and P.Breeden, 1994: Segmentation of polar scenes using multispectral texture measures and morphological filtering. *Int. J. Rem. Sens.*, **15**, 1019 - 1036

Coakley J.A. Jr and F.P. Bretherton 1982: Cloud cover from high-resolution scanner data:Detecting and allowing for partially filled fields of view, *J. Geophys. Res.* ,**87**, 4 917 - 4 932.

Ebert, E., 1987: A pattern recognition technique for distinguishing surface and cloud types in polar regions. *J. Clim. Appl. Meteor.*, **26**, 1412 - 1427.

Garrand, L. 1988: Automated recognition of oceanic cloud patterns. Part I: Methodology and Application to cloud climatology. *J. Climate*, **1**, 20 - 39.

Gutman, G.G., 1992: Satellite daytime image classification for global studies of Earth's surface parameters from polar orbiters. *Inn. J. Rem. Sens.* **13**, 209 - 234.

Hildebrand, P.H. 1978: Iterative correction for attenuation of 5 cm radar in rain. *J. Appl. Meteor.* , **17**, 508 -513.

Hou, Y-T, K.A. Campana, K.E. Mitchell, S-K Yang and L.L. Stowe, 1993: Comparison of an Experimental NOAA AVHRR Cloud Dataset with Observed and Forecast Cloud Datasets. *J. Atmos. Oceanic Tech.*, **10**, 833-849.

Hunt, G.E., 1973: Radiative properties of terrestrial clouds at visible and infrared thermal window wavelengths. *Q. J. Meteorol. Soc.*, **99**, 346 - 369

Inoue , T. 1985: On the temperature and effective emissivity determination of semi-transparent cirrus clouds by bi-spectral measurements in the 10 μm window region. *J. Met. Soc. Japan*, **63**, 88 - 99.

Kidson, J., J. Couper, and M. Uddstrom, 1992: Interactive visualization at the New Zealand Meteorological Service. In the proceedings of *Eighth International Conference on Interactive Information and Processing Systems for Meteorology, Oceanography, and Hydrology*, Atlanta, Georgia, USA. Pub. AMS. 132 -134.

Lovejoy S. and G.L. Austin, 1979: The delineation of rain areas from visible and IR satellite data for GATE and mid-latitudes. *Atmos. Ocean*, **17**, 77 - 92.

Molnar, G. and J.A. Coakley, Jr. 1985: Retrieval of cloud cover from satellite imagery data; A statistical approach, *J. Geopyhs. Res.* **90**, 12 960 - 12970.

Murphy, A.H., and R.W. Katz: *Probability, statistics and decision-making in the atmospheric sciences.*

Olesen, F.-S., and H. Grassl: 1985: Cloud detection and classification over oceans at night with NOAA-7. *Int. J. Rem. Sens.*, **6**, 1435 - 1444.

Parikh, J., 1977: A comparative study of cloud classification techniques. *Rem. Sens. Env.*, **6**, 67 - 81.

Planet, W.G. (Ed), 1988: Data extraction and calibration of TIROS-N/NOAA Radiometers. *NOAA Tech. Memo. NESS 107 - Rev 1.*

Rosenfeld, D. and G. Gutman, 1994: Retrieving microphysical properties near the tops of potential rain clouds by multispectral analysis of AVHRR data. *Atmos. Res.*, **34**, 259 - 283.

Saunders R.W. and K.T. Kriebel, 1988: An improved method for detecting clear sky and cloudy radiances from AVHRR data. *Int. J. Rem. Sens.*, **9**, 123 - 150.

Stephens, G.L., and T.J. Greenwald 1991: The Earth's radiation budget and its relation to atmospheric hydrology:2. Observations of cloud effects. *J. Geophys. Res.* **96**, 15 325 - 15 340.

Stowe L.L., E.P. McClain, R. Carey, P. Pellegrino, G.G. Gutman, P. Davis, C. Long and S. Hart. 1991: Global distribution of cloud cover derived from NOAA/AVHRR operational satellite data. *Adv. Space Res.*, **11**, (3) 51 - 54.

Tovinkere, V.R., M. Penaloza, A. Logar, J. Lee, R.C. Weger, T.A. Berendes and R.M. Welch 1993: An intercomparison of artificial intelligence approaches for polar scene identification. *J. Geophys. Res.* **98**, 5001 - 5016

Tukey, J.W., 1977: *Exploratory Data Analysis.* Reading, Mass: Adison-Wesley.

Welch R.M., S.K. Sengupta, K.S. Kuo 1988: Marine stratocumulus cloud fields off the coast of southern California observed using LANDSAT imagery. Part II: Textural analysis. *J. Appl. Meteor.*, **27**, 363 - 378.

Weszka, J.S., C.R. Dyer, and A. Rosenfeld, 1976: A comparative study of texture measures for terrain classification. *IEEE Trans. Syst. Man. Cybern.*, **SMC-6**, 269 - 285.

Wright B.J. and B.W. Golding, 1990: The interactive mesoscale assimilation., *Met. Mag.* **119**, 234 - 243.

Wu, R., J.A. Weinman, R.T. Chin, 1985: Determination of rainfall rates from GOES satellite images by a pattern recognition technique. *J. Atmos. Oceanic Tech.*, **2**, 314 - 330.

TECHNICAL PROCEEDINGS OF

THE EIGHTH INTERNATIONAL TOVS STUDY CONFERENCE

Queenstown, New Zealand

5-11 April 1995

Edited by

J R Eyre

Meteorological Office, Bracknell, U.K.

Published by

European Centre for Medium-range Weather Forecasts
Shinfield Park, Reading, RG2 9AX, U.K.

July 1995